Joint Special Interest Group meeting between euspen and ASPE
Advancing Precision in Additive Manufacturing
TU Berlin, Germany, October 2025
www.euspen.eu

Comparison of laser powder bed fusion fatigue bar surfaces measured with laser confocal microscopy and X-ray micro CT using both traditional and neural network based reconstructions

Edwin B Glaubitz[1], Nathan S Johnson[2], Joy Gockel[1]

[1] *Colorado School of Mines, 1500 Illinois St. Golden, Colorado 80401, USA*
[2]*Carl Zeiss Inc. Zeiss Innovation Center, 5300 Central Parkway Dublin, CA 94568, USA*

glaubitz@mines.edu

Abstract
Surfaces of components built using laser powder bed fusion (PBF-LB) are rougher than those made using traditional manufacturing techniques. Unique surface features: adhered particles, weld tracks, layering artifacts, and surface notches make characterizing and understanding surfaces more difficult. Modifying the surface roughness through post processing is potentially impractical due to the complex geometries that can be produced with the process. Laser confocal scanning microscopy (LCSM) is an optical 3d measurement technique which is capable of high resolution and repeatable surface roughness measurements, but cannot practically measure very large regions due to the need for stitching. X-Ray micro computed tomography (microCT) is a technique that generates a volumetric pixel (voxel) reconstruction of an object from many x-ray radiographs of the object at different rotations. This technique can image complex geometries without the limitations of LCSM but, high resolution CT scanning is extremely costly. Neural network based image enhancement techniques have recently become more popular as computer hardware has evolved to include dedicated neural processors and higher power graphics processing and have been recently applied to reconstruction of microCT data. Surface roughness measurements on a standard fatigue bar geometry made from 316L stainless steel are collected using three techniques: LCSM, low-res microCT, and enhanced resolution microCT using a neural network trained on a high resolution small area scan of the fatigue bar. Differences in commonly reported surface roughness metrics are characterized. Surface notch defects in each data set are identified and characterized to compare them with defect measurements from fatigue failed bars from the same build. Conclusions are made on the influence of measurement technique and resolution on defect measurements and fatigue life predictions.

Laser Powder Bed Fusion, Surface Roughness, microCT, Confocal Microscopy, Fatigue

1. Introduction

Laser Powder Bed Fusion (PBF-LB) is an additive manufacturing process that builds components by selectively melting powder layers using a laser. Surface roughness of as-built components can vary due to process parameters [1–3], build location and orientation [4], and other factors. 316L stainless steel is a particular alloy of interest as the unique processing conditions of the PBF-LB process can lead to overall higher tensile properties than wrought [5]. However, as-built surface roughness, and primarily valleys/notches in the surface have been linked to lower fatigue performance compared to additive and wrought material with machined surfaces [6–9].

Achieving consistent measurements of as-built roughness is difficult since measurements vary across different part locations, and different measurement techniques [10]. One source of variation is the differences in resolution across measurement techniques: laser scanning confocal microscopy (LCSM) has a resolution that is typically in the micron to sub-micron scale which is possible but often impractical for laboratory-based X-ray micro computed tomography (microCT).

Use of neural networks to produce enhanced images is a relatively new development thanks to ever more powerful computer hardware and development of better neural models [11]. Enhancing X-ray images using this process has also been of interest since the high time and resource cost of the image acquisition process could be reduced through image enhancement [12,13]. In traditional laboratory X-ray CT, large volume high resolution datasets are constructed by stitching together many high resolution sub volumes. This requires long acquisition times and the collection of many data sets. Neural network based image recovery technique can generate high resolution, large volume datasets from just two X-ray CT scans.

This work will examine the surface roughness of an as-built PBF-LB manufactured 316L stainless steel fatigue bar with three different surface roughness measurement techniques: LCSM, microCT, and enhanced resolution microCT using a neural network trained on a high-resolution scan of the same fatigue bar. Test bars that have different surface roughness due to process conditions will be compared across the different measurement techniques. Surface notch data from a wider experiment will be discussed in the context of creating more accurate and transferrable surface roughness measurements.

2. Methods

2.1. Fatigue Bar Fabrication

Fatigue bars were fabricated using a 3DSystems DMP Flex 350 PBF-LB machine using 316L stainless steel. The test bars were designed with a 6 mm diameter, and 12 mm long cylindrical gauge section which is one of the recommended sizes in ISO 1143 [14]. A 60 µm layer height was selected and process parameters known to produce large stochastic surface notches that initiate fatigue failure were selected and are shown in **Table 1** and were scanned in the following order bulk, inner contour,

outer contour. In the build chamber, 120 fatigue bars were fabricated in total with 60 being fabricated with the surface notch parameter set.

Table 1 Process Parameters for 316L Stainless Steel Fatigue Bars

Scan Strategy Name	Bulk/infill	Inner Contour	Outer Contour
Laser Power, W	300	300	150
Scan Speed, mm/s	900	800	450
Offset Inside of Slice Boundary, µm	150	150	63
Hatch Spacing, µm	100	N/A	N/A

2.2. Laser Scanning Confocal Microscope Measurements and Processing

Laser Scanning Confocal Microscope (LCSM) measurements were collected on an Olympus OLS5100 using a 50x magnification long working distance lens with a numerical aperture of 0.6 and a pixel size of 0.256 µm. This lens was higher magnification than necessary but selected because the other lenses may have collided with the specimens due to the geometry. Each scan comprised of a stitched area 1.4 mm wide by 1.4 mm tall which was chosen as it was the largest area that could be acquired without the microscope software down sampling the results. To make up for the small scan area, two scans were collected from each region of the fatigue bars. Regions on the fatigue bars were defined based on their orientation in the build chamber: region A is oriented away from the across-bed gas flow, B faces the recoating axis, C faces the across-bed gas flow, and D also faces the recoating axis but is on the opposite side from B. Each of these regions is 90 degrees clockwise from the previous region when viewed from the top of the build down. Nearly the entire population of fatigue bars manufactured during the build had two scans taken on region A which often has the highest roughness. The bar that was selected for microCT measurement had regions A, B, C, and D scanned since the microCT would be able to image the entire gauge section.

After scanning, the 3d surface data was exported to a CSV file for processing in the commercial areal roughness software OmniSurf3D[15]. Scans were processed with cylinder form removal, short wavelength cutoff at 2 µm, and long wavelength cutoff at 1.4 mm in both cases the robust gaussian filter was used due to its better handling of step height changes, such as those found around adhered powder particles. Surface roughness metrics were calculated from the filtered surface.

2.3. MicroCT Measurements and Data Processing

X-ray microscopy (microCT) datasets were collected using a ZEISS 630 VersaXRM (ZEISS, Dublin, CA) with a 160kV source voltage and 25W source power. The source was placed as close to the sample as possible to maximize transmission through the sample. All scans were collected using the ZEISS proprietary HE6 filter.

Two datasets were collected to train the deep learning model. First, a large field of view (LFOV) dataset, encompassing the entire gauge region, was collected using a 0.4X magnifying objective with a nominal pixel size of 8 microns, and a sample-to-detector distance of 220mm. Then, a high resolution (HR) 'zoom' dataset was collected on a sub-region of the gauge using a 4X magnifying objective with a pixel size of 1.8 microns and a sample-to-detector distance of 45mm. All datasets were collected with 2401 projection radiographs.

The LFOV and HR datasets were used to train the DeepScout (DS) model (ZEISS Advanced Reconstruction Toolbox v4.0) which is an image superresolution technique based on the noise-to-noise Unet architecture [11]. Training and inference were performed on a workstation with 512 GB RAM and an Nvidia RTX 6000 Ada generation GPU. The final pixel size of the DS reconstructed volume was 1.8 microns.

The reconstructed data was segmented using a manually selected threshold value. The four regions of the gauge section were cropped out using a 3 mm wide selection box which was approximately 6 mm tall (slightly shorter than the reconstructed volume) and as deep as necessary to collect the entire surface. Each region was meshed and exported as a STL file. Regions were then imported into OmniSurf3d and processed using cylinder form removal, short wavelength cutoff at 2 µm, and long wavelength cutoff at 1.4 mm. Surface roughness metrics were calculated from the filtered surface. The same long wavelength cutoff was used to be consistent with the LCSM measurement. The assumption was made that the extra processing steps for reconstructing both the LFOV and DS volumes would similarly be sufficient to denoise the image so the same 2 µm short wavelength cutoff was used for them.

3. Results

The surface roughness measured by the three methods: LCSM, LFOV and DS varied across the regions with some metrics being more in agreement across the methods than others. Measurement of average surface roughness (Sa) was very similar between the LCSM and DS techniques for regions A, B, and C, while in region D, the DS reconstruction measured a lower Sa than the LFOV reconstruction. An unexpected result was that the LFOV data greatly undermeasured Sa compared to the LCSM and DS for sides A and B while C and D were more similar. Sa measured by each of the techniques for the different regions is shown in **Figure 1**.

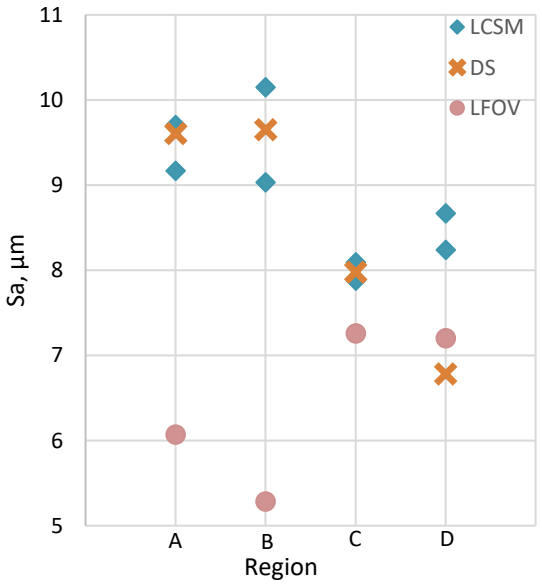

Figure 1. Sa vs region on the fatigue bar for the LCSM, DS, and LFOV measurement techniques

Surface maximum valley (Sv) measurements shown in **Figure 2** had different results across the measurement techniques than the Sa results. In some cases, the Sv measured in the LCSM and LFOV techniques were within a couple microns, while the DS measurement of Sv was always higher and only close to either the LCSM or LFOV measurement in one case.

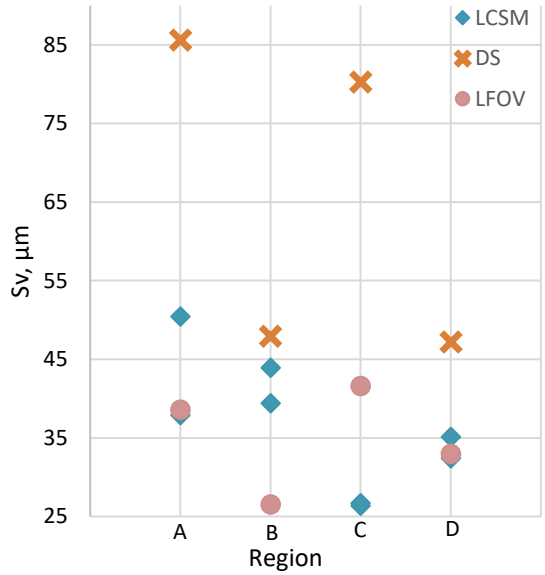

Figure 2. Sv vs region for the LCSM, DS, and LFOV measurement techniques

Other roughness metrics like root mean square roughness (Sq) and skewness (Ssk) can be used to understand some of the properties of the distribution of heights measured by each technique since Sq is also the standard deviation and Ssk characterizes whether the distribution has more values above or below the mean surface. The Ssk measurements illustrated in **Figure 3**, shows the LCSM always measured higher than LFOV and DS and across the different regions, and there was no consistent relationship across the techniques. The Sq measurements in **Figure 4** were similar to the Sa measurements, however in region C the DS measurement was lower than the LCSM measurements where it was between the LCSM measurements for Sa.

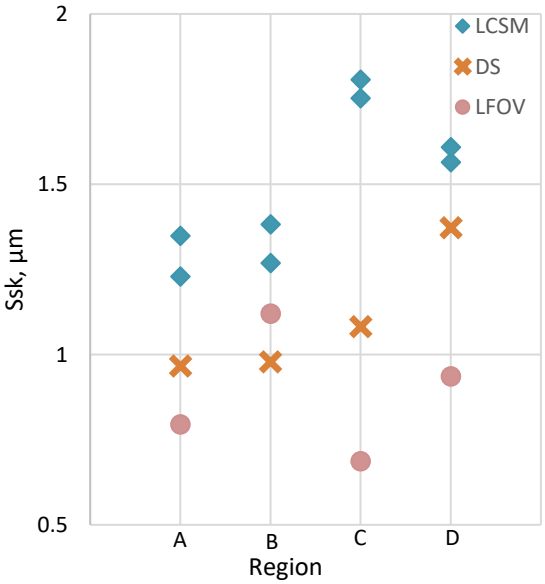

Figure 3. Ssk vs region for the LCSM, DS, and LFOV measurement techniques

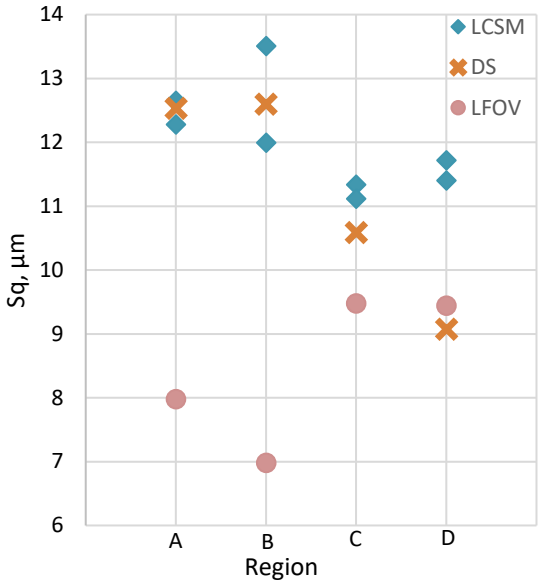

Figure 4. Sq vs region for the LCSM, DS, and LFOV measurement techniques

4. Discussion

The results showed that in regions A, B, and C, the DS reconstruction surfaces had similar Sa surface roughness values to those measured using LCSM and higher roughness than the LFOV measurement which is possibly too low of a resolution to resolve the adhered powders which contribute to the high average roughness. Inconsistency in the Sa measurement in region D appears to be due to acquisition settings since the surface was not as clearly imaged in this region. Sq and Ssk, which indicate the standard deviation and skewness of the distribution of height measurements show that while the Sa is similar, the distributions are not. The Sq of the DS reconstruction was lower than the LCSM for region C when the Sa was almost perfectly between the two LCSM measurements. This is likely due to less peaks being in the data since Sq will weight extreme values more than Sa and the Ssk of region C showed that the DS reconstruction was much lower than the LCSM, which indicates that the tail of the distribution corresponding to surface peaks was not as large.

The characterization of the largest surface valley through the Sv parameter shows that the DS reconstruction consistently measures a higher value compared to the LCSM. The cause of this is that the LCSM measurements did not contain surface valleys as large as the ones that appear in the much larger microCT measurements. The fatigue bars have abnormally large surface notch defects that are very spread out so the measurement area becomes a major factor in the results. Since the microCT measurements cover a much larger proportion of the gauge section than the LCSM measurements, the probability of observing a surface notch defect increases. Cropping the DS dataset down to a 1.4 mm square measurement area like the one produced by the LCSM showed that in many cases a lower value of Sv was measured. Registration of these data sets to make direct measurement comparisons could not be performed since adding fiducial markings was not practical in this case. Initial work manually registering the data through the unique patterns of adhered particles is being explored.

Across a wider sample of the fatigue bars made using this parameter set, there was an interesting result when looking at the population of Sv measured by LCSM, the notch depth from post fatigue-failure fractography, and the microCT measurements from the single fatigue bar. The population of

LCSM measurements has a bimodal distribution where the left peak, centered on 35 µm Sv measurements without an abnormally large surface notch, and the other peak represents measurements that have a surface notch. The measured failure initiating notch depth from fractography overlaps the distribution of Sv measurements with a surface notch which indicates that the LCSM is getting good measurements of notch depths when one exists in the measurement area. The microCT data on the other hand covers around half of the total gauge section length which greatly increases the chances of seeing a large surface notch in the measurement area. The LFOV measurement is well outside the distribution of failure initiating notches while the DS measurement is not, which means that DS could be better at characterizing notches than the LFOV. The DS is within the range of expected notches for the population of fatigue bars made in this build with the same parameters. The distributions of Sv and failure initiating notch measurements is shown in **Figure 5**.

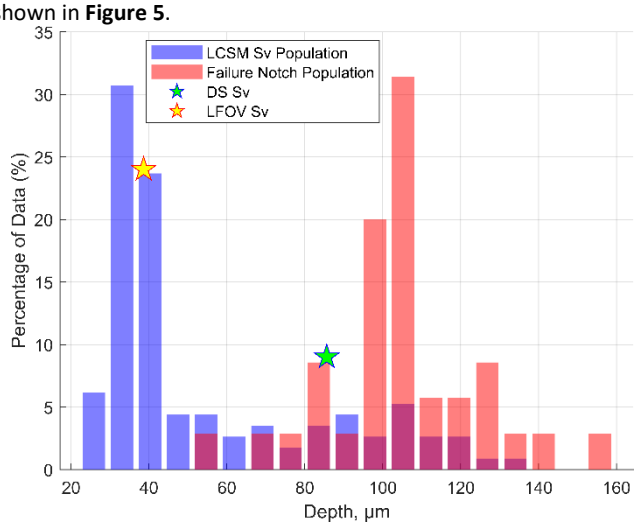

Figure 5. Populations of Sv from region A on 57 fatigue bars and failure initiating notch measurements from the tested bars

5. Conclusions

The following conclusions were drawn from the analysis of the data collected for this work:

- Sa measured using the DS reconstruction was comparable to Sa measured using LCSM.
- The DS reconstruction had a higher Sv than the LCSM measurements due to the larger measurement area having a higher likelihood of containing a surface notch
- Despite the comparable Sa, the DS reconstruction is not identical to the LCSM since the Sq and Ssk metrics are very different.
- The DS measurement of Sv is closer to the expected notch depth than the LFOV Sv

References

[1] E.B. Glaubitz, J.C. Fox, O.L. Kafka, J. Gockel, Contour parameters, melt pool behavior, and surface roughness relationships across laser powder bed fusion platforms and metallic alloys, Int J Adv Manuf Technol (2025). https://doi.org/10.1007/s00170-025-15066-0.

[2] A. Kleen, E. Glaubitz, J. Gockel, The Influence of Contour Offset in Laser Powder Bed Fusion on Melt Pool Behaviors, Surface Roughness, and Sub-Surface Porosity, in: University of Texas at Austin, 2024. https://doi.org/10.26153/TSW/58089.

[3] O.L. Kafka, J. Benzing, N. Derimow, P. Schumacher, L. Koepke, C. Beamer, D. Godfrey, N. Hrabe, Effects of as-built surface with varying number of contour passes on high-cycle fatigue behavior of additively manufactured nickel alloy 718, International Journal of Fatigue 176 (2023) 107872. https://doi.org/10.1016/j.ijfatigue.2023.107872.

[4] J.C. Fox, S.P. Moylan, B.M. Lane, Effect of Process Parameters on the Surface Roughness of Overhanging Structures in Laser Powder Bed Fusion Additive Manufacturing, Procedia CIRP 45 (2016) 131–134. https://doi.org/10.1016/j.procir.2016.02.347.

[5] N. Ahmed, I. Barsoum, G. Haidemenopoulos, R.K.A. Al-Rub, Process parameter selection and optimization of laser powder bed fusion for 316L stainless steel: A review, Journal of Manufacturing Processes 75 (2022) 415–434. https://doi.org/10.1016/j.jmapro.2021.12.064.

[6] A. Avanzini, Fatigue Behavior of Additively Manufactured Stainless Steel 316L, Materials 16 (2022) 65. https://doi.org/10.3390/ma16010065.

[7] M. Braun, E. Mayer, I. Kryukov, C. Wolf, S. Böhm, A. Taghipour, R.E. Wu, S. Ehlers, S. Sheikhi, Fatigue strength of PBF-LB/M and wrought 316L stainless steel: effect of post-treatment and cyclic mean stress, Fatigue Fract Eng Mat Struct 44 (2021) 3077–3093. https://doi.org/10.1111/ffe.13552.

[8] S. Hatami, T. Ma, T. Vuoristo, J. Bertilsson, O. Lyckfeldt, Fatigue Strength of 316 L Stainless Steel Manufactured by Selective Laser Melting, J. of Materi Eng and Perform 29 (2020) 3183–3194. https://doi.org/10.1007/s11665-020-04859-x.

[9] S. Richardsen, G.H. Crawford, J. Gockel, Effect of a build pause on the fatigue behavior of laser powder bed fusion 316L stainless steel with as-built surfaces, Engineering Failure Analysis 153 (2023) 107590. https://doi.org/10.1016/j.engfailanal.2023.107590.

[10] E. Glaubitz, O. Kafka, J. Fox, J. Gockel, MEASUREMENT OF LASER POWDER BED FUSION SURFACES USING NON-CONTACT TECHNIQUES, in: Golden, Colorado, USA, 2024.

[11] J. Lehtinen, J. Munkberg, J. Hasselgren, S. Laine, T. Karras, M. Aittala, T. Aila, Noise2Noise: Learning Image Restoration without Clean Data, (2018). https://doi.org/10.48550/arXiv.1803.04189.

[12] M. Andrew, A. Andreyev, F. Yang, M. Xu, S. Xu, X-ray reconstruction using synthetic prior image restoration, with application to noise and artefact removal, in: B. Müller, G. Wang (Eds.), Developments in X-Ray Tomography XV, SPIE, San Diego, United States, 2024: p. 12. https://doi.org/10.1117/12.3027813.

[13] M. Andrew, L. Omlor, A. Andreyev, R. Sanapala, M. Samadi Khoshkhoo, New technologies for x-ray microscopy: phase correction and fully automated deep learning based tomographic reconstruction, in: B. Müller, G. Wang (Eds.), Developments in X-Ray Tomography XIII, SPIE, San Diego, United States, 2021: p. 15. https://doi.org/10.1117/12.2596592.

[14] ISO 1143:2021, (n.d.).

[15] OmniSurf3D, (n.d.). https://digitalmetrology.com/solution/omnisurf3d/.